Efficient Design of Photonic Integrated Circuits

Cristina Arellano, Sergei Mingaleev*, Eugene Sokolov*, Igor Koltchanov, *Member, IEEE*
and André Richter, *Senior Member, IEEE*
VPIsystems GmbH, Carnotstr. 6, 10587 Berlin, Germany
**VPI Development Center, Chapaeva str. 5, 220034 Minsk, Belarus*
Tel: +49 30 398 0580, Fax: +49 398 05858, e-mail: Cristina.Arellano@VPIsystems.com

ABSTRACT
The exponentially growing number of components in complex large-scale Photonic Integrated Circuits (PICs) requires the necessity of photonic design tools with system-level abstraction. This work addresses the modeling of large-scale integrated PICs from a system-level perspective. Behavioral models of ring resonators, multimode interference devices, optical waveguides and other fundamental building blocks of PICs will be presented and combined to demonstrate several application examples of photonic circuit designs.
Keywords: photonic integrated circuit, photonic waveguide, scattering matrix, design, modeling.

1. INTRODUCTION

The competence to integrate a large number of optical elements on single wafer-dices is currently one of the main research objectives for data communications and networking applications. The number of sub-components in Photonic Integrated Circuits (PICs) increases exponentially, similar as predicted by Moore's law for electronic integrated circuits raising the demand for efficient and powerful PIC design software tools. Traditional simulators of photonic devices are based on solving the Maxwell equations, referring for example, the Finite-Difference Time-Domain method [1] or the Beam-Propagation method [2] as the most frequently used. The computational effort associated with this type of simulators increases significantly with the number of photonic elements employed in the modeled structure making their application for complex large-scale PICs often unfeasible. Physical design parameters of the PIC under investigation (for example, material, insertion loss, power, birefringence, temperature, electronic driving circuit) impact directly the system to be deployed later. Modeling of photonic integrated circuits from a system perspective may solve questions like what is the performance of the integrated circuit sub-system or how does the sub-system performance affect the system. The system-level abstraction for modeling large-scale PICs reported in this and previous works [3], overcomes the above limitations and can be used to accurately model integrated components comprising tenths of elements, such as ring-resonators, ring-couplers, x-couplers or multimode interference (MMI) devices, in a single design. Moreover, our modeling approach permits the optimization of individual photonic elements to enhance the performance of the modeled system as a whole.

2. MODELING FRAMEWORK FOR PHOTONIC INTEGRATED CIRCUITS

Modeling speed can be increased significantly with frequency-domain simulations. Most of the basic PIC sub-components are passive and do not require a deep level of detail and can be described in terms of frequency-defined S-matrices. The S-matrix approach has been developed long ago and is widely used in high-frequency electrical engineering to characterize and design microwave circuits. This method can also be applied for the modeling of large-scale photonic crystals [4-5].

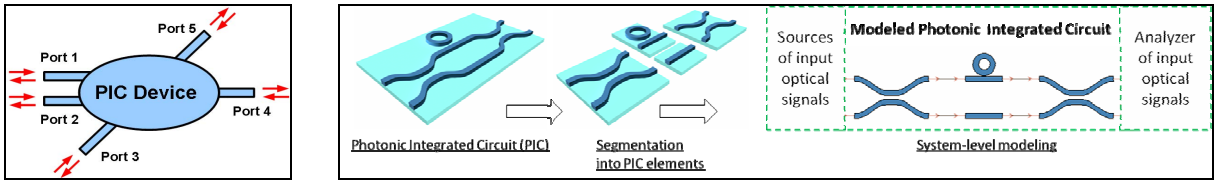

Figure 1. Representation of a 5-port PIC device (left);system-level modeling approach implemented in VPIcomponentMaker Photonic Circuits 8.6

Towards the S-matrix method, in our modeling framework, each device is considered as a black box, characterized by several ports, enumerated from 1 to N (Fig. 1). Each port represents a device connection point where optical signals enter/exit the device. In most cases, ports can be associated with photonic connection waveguides. The resulting S-matrix of the modeled passive PIC device is a matrix of complex frequency-dependent functions (transfer functions) that is multiplied in frequency domain (or convolved in the time domain) with the input signals producing the output signals. In that way, photonic circuits are assembled from basic building blocks simulating the characteristics of geometrical structures, each of them being represented by its S-matrix (Fig. 1). PICs might also comprise active devices such as semiconductor lasers, amplifiers, or

absorbers, which are modeled favourably in the time domain by means of the Transmission-Line Laser Model (TLM)[6]. Active and passive elements can interoperate in a same simulation schematic however we focus in the following application examples on pure passive PICs. The identified key building blocks are also illustrated in Fig. 1.

3. APPLICATION EXAMPLES

3.1 Multiple ring-loaded Mach-Zehnder Structure

The first discussed application example is a modulator consisting of a Mach-Zehnder interferometer (MZM) loaded with cascaded ring resonator elements (Fig. 2). This type of device presents better modulation efficiency when compared with a conventional MZM having a similar footprint size [7]. Here we want to point out that the design of a device with a large number of complex elements (in this case: a total of 22) does not imply a huge degree of complexity in editing or analyzing the design. Fig. 3 (top) shows corresponding transfer functions at output ports over a large spectral range. The ring-resonator structure consists of an optical waveguide bended into a circle and placed close to a straight waveguide, such that coupling between these two elements occurs. The resultant magnitude of the transfer function equals unity for all frequencies while its group delay has maxima at resonance frequencies so it acts as an all-pass phase shifter. The resonance frequencies are determined by the length of the waveguide forming the ring. The analytical description of its S-matrix is determined on the basis of physical parameters [8], either for getting the desired resonance properties (specified by the Free Spectral Range – FSR, design polarization, resonance frequency, and Q-factor) or on the basis of structure parameters (specified by parameters such as coupling waveguide-ring, ring length and ring phase shift).

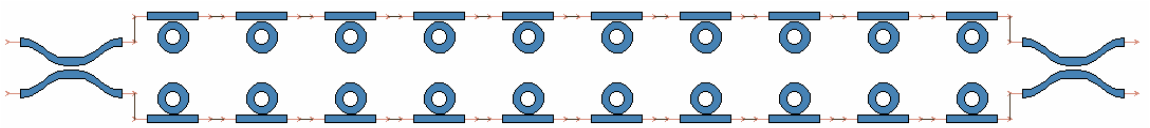

Figure 2. Schematic of the 10-cascaded ring-loaded Mach-Zehnder device.

Effective and group indices might differ for different polarizations; in fact, they are very different in bulk silicon devices compared to devices developed in silicon-on-insulator (SOI). Exemplary, Fig. 3 (bottom) shows group delay for TE and TM polarizations of the same device considering different values of group and effective indices for the two polarizations. This case illustrates the different constellation of resonance frequencies what might impact severely polarization-multiplexed systems, for instance, and should be taken into account in the system design. The degree of degradation of the system might be further investigated by systematic numerical simulations.

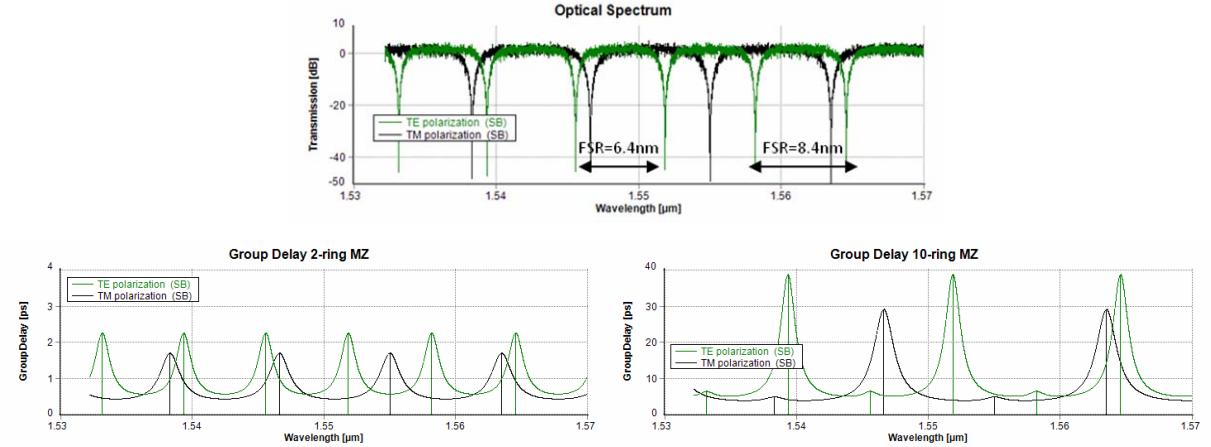

Figure 3. Magnitude of the transfer function at output ports for TE and TM polarizations (top); group delay for a 2-ring MZM and 10-ring MZM (bottom).

In such a structure, modulation is accomplished by utilizing the electro-optical thermal effect, where electric carriers are injected from the electrodes inducing changes in the refractive index. In order to analyze the modulation capabilities, this effect is mimicked in our model for a different number of active rings. The eye diagrams represented in Fig. 4 show that in our example, the extinction ratio is optimum for eight active rings and distorted in the case of more than ten rings.

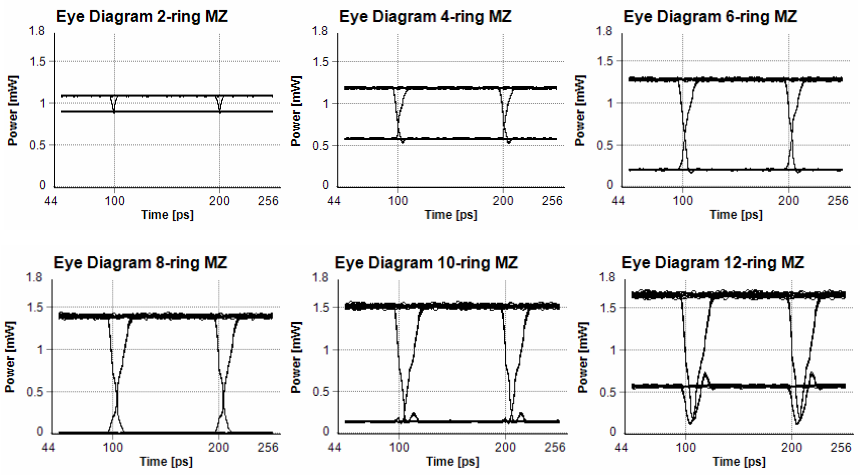

Figure 4. Eye diagrams for different number of active rings

3.2 All-optical nonlinear switching in micro-ring resonator

One of the most compact all-optical nonlinear switches consists of a waveguide-ring resonator with a micro-ring formed by a highly nonlinear waveguide. Here, we consider an all-optical dynamic tuning approach that is based on the usage of nonlinear waveguides in high-Q resonant systems, where the refractive index is dynamically tuned during the simulation duration. The basic characteristics of this device are taken from the first experimental demonstration of all-optical switching in GaAs-AlGaAs structure reported in [9].

In the schematic below (Fig. 5), the linear transmission spectrum through the 10-micron-radius ring-resonator structure exhibits periodically repeated (with free spectral range 1.35 THz) resonant absorption dips, in particular at 193.1 and 194.45 THz. If only the low-intensity probe pulse at resonant frequency 194.45 THz is transmitted, it is strongly attenuated and does not pass to the output. However, in the case of transmitting a probe pulse together with the moderate-power pump pulse at 193.1125 THz (blue-shifted by 12.5 GHz from the resonant frequency) the field is significantly enhanced inside the micro-ring. This decreases the effective index by about 0.0002 and thus, causes a blue shift of all resonant frequencies by about 12.5 GHz. In such a situation, the probe pulse is already out-of-resonance and passes to the output.

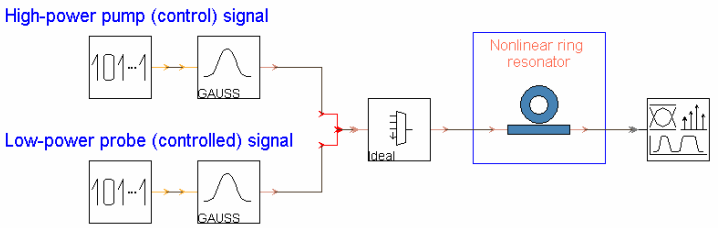

Figure 5. Schematic of the micro-ring resonator nonlinear switch.

Results for a nonlinear coefficient of -0.0002 W^{-1} and attenuation in the ring of 7000 dB/m are represented in Fig. 6 (left) where the transmission of the probe pulse is switched on by sending a pump pulse during the time slot. In the absence of waveguide nonlinearity probe pulses would be significantly attenuated, independently on the presence/absence of the pump pulse. Fig. 6 (right) represents the importance that the device has strong attenuation. In the absence of attenuation, the pump signal is still present at the output and the on/off states cannot be distinguished clearly.

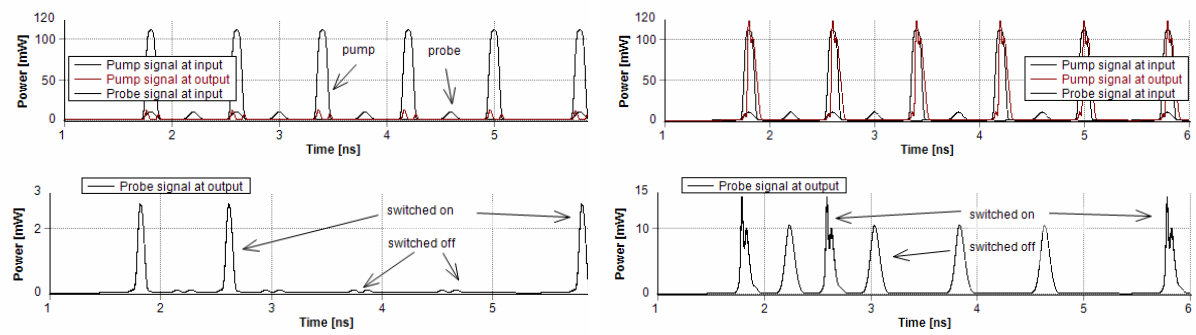

Figure 6. Waveform of pump and probe signals at input and output ports for strong attenuation inside the ring (left) and no attenuation inside the ring (right).

3.3 Coherent optical receiver

One of the main elements within a coherent optical receiver is the 90-degree hybrid, which is responsible for separating the modulated signal into its in-phase (I) and quadrature (Q) components. In novel integrated receivers, such function is accomplished by a specifically designed MMI device [10]. The MMI-based 90-degree hybrid is designed from a 4x4-MMI device where only two of the input ports are used [11]. For MMI devices, S-parameters can be calculated analytically using the Self-imaging Matrix model [12]. Once the total width, dimension and position of ports are defined, the model calculates the optimum length (see in the top of Fig. 7 the internal field distribution when illuminating one of the input ports). A point-to-point coherent system is represented in Fig. 7 (bottom). The signal composed by I and Q components is input to the MMI and mixed there with the local oscillator. Signals at the outputs of the MMI are then photo-detected and combined to recover its I and Q parts. Typical effects such as tolerances of ports widths or ports position can be easily analyzed in this setup. For instance, in the chart in Fig. 7 is represented the eye closure of the detected signals when the MMI width is tuned from its original value, showing a severe impact for relative small increments in the width.

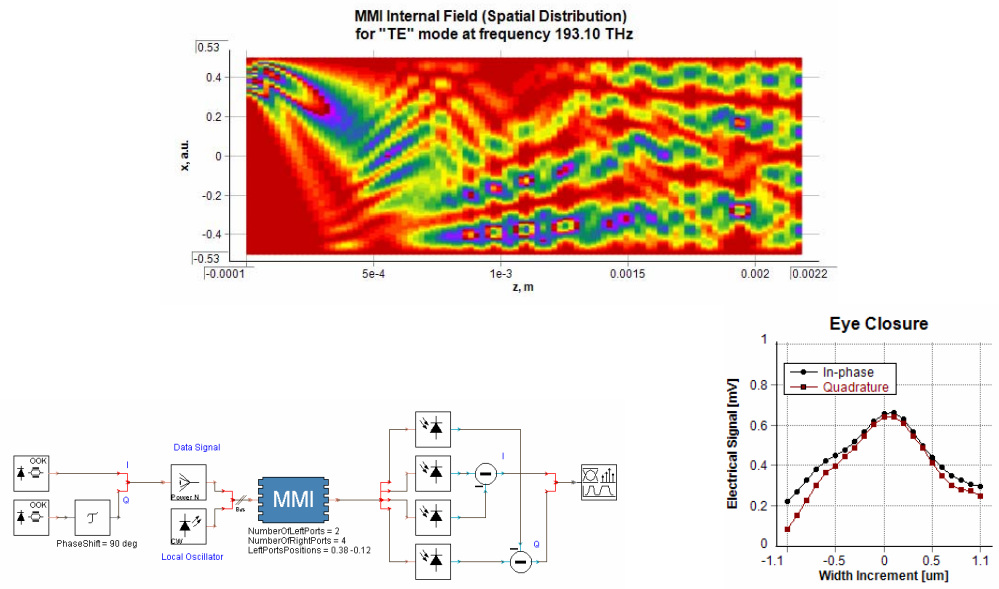

Figure 7. Distribution of the internal field in the MMI for one input illuminated (top). Schematic of the coherent receiver and effects in the eye closure when tuning the MMI width from the optimum value (bottom).

3.4 Design and optimization of Arrayed Waveguide Grating

This example illustrates the design of an Arrayed Waveguide Grating (AWG) built from star coupler and optical waveguide elements. In this case, the Multi-grating method is used to obtain a flattened spectral response [13]. Within this approach, the grating between star couplers is separated into two sub-gratings where each has its own length increment and central wavelength. If these wavelengths are slightly different, the final spectral response is flattened. The analytical model for star coupler elements is based on field transformation through a finite Fourier transform. S-parameters are calculated analytically in paraxial approximation using the Fourier optics model. S-parameters for straight waveguides are calculated on the basis of waveguide length, attenuation, mode coupling coefficient, effective index and group mode indices and dispersion. The spectra of the 16 output ports of the 1x16 AWG multiplexer still without optimization are represented in Fig. 8 (left). First, uniform-distributed random variations of the phase shift in the waveguides are introduced in the model. In Fig. 8 (right) it can be verified that the presence of the simulated phase errors leads to higher AWG crosstalk, although other AWG characteristics remain almost unchangeable.

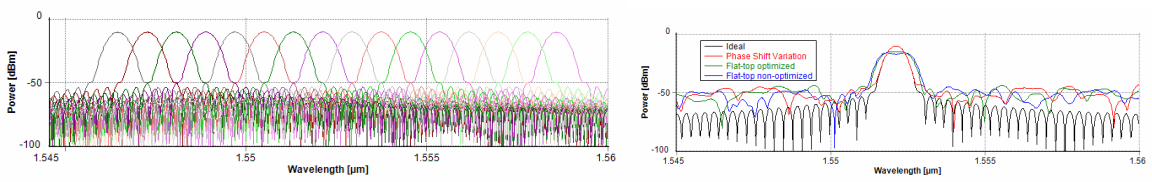

Figure 8. Spectra of the 16-channel AWG output ports (left); spectra of the central channel at the output for flat-optimized and non-optimized cases

The increment of the length at the waveguides is described as *Length Increment±0.5Increment Difference*, for even and odd waveguides, correspondingly. Tuning the value of the incremental difference leads to inconstant

length increments. Consequently spectral responses for even and odd gratings shift to the lower and higher frequencies respectively. An optimum value can be found such that the spectral responses are flattened. Fig. 8 (right) shows that the spectral response is flattened for the optimized AWG, whilst it presents peaks for values that differ from the optimum one. Note also that the insertion loss rises, which is typical in flat-top multiplexers.

4. CONCLUSIONS

Lead by the necessity for photonic design tools with system-level abstraction that support efficient simulations we have developed a simulation framework for photonic integrated circuits in the context of the professional design suite *VPItransmissionMaker/VPIcomponentMaker*. Among others, it offers a family of passive PIC elements and provides efficient numerical simulation of passive elements and circuits based on the S-matrix approach. Accurate analytical models (e.g., self-imaging matrix for MMI devices, paraxial approximation using the Fourier optics model for star couplers, and other methods) grant the optimization of designs in terms of tolerances due to random variations of phase shift or dimensions. Different values of effective and group indices and of TE and TM modes are supported in the analytical models to investigate polarization coupling and dispersion effects in waveguide-based elements. We presented application examples of PICs that contain ring-resonators, MMI devices, AWG and photonic waveguides as fundamental structures. The presented examples enclose passive elements only allowing numerical simulations to be carried out entirely in the frequency-domain. The discussed level of modeling PICs allows a seamless integration with systems-level simulation techniques.

ACKNOWLEDGEMENTS

The research leading to these results has received funding from the European Union Seventh Framework Program FP7/2007-2013 under grant agreement n° 257980 (MIRTHE).

REFERENCES

[1] A. Taflove and S. C. Hagness, *Computational Electrodynamics: The Finite-Difference Time-Domain Method*, 3rd ed. (Norwood, MA: Artech House, 2005).

[2] K. Kawano, T. Kitoh: Beam Propagation Methods, in Introduction to Optical Waveguide Analysis: Solving Maxwell's Equations and the Schrödinger Equation (Wiley, NY, 2002).

[3] C. Arellano, S. Mingaleev, E. Sokolov, I. Koltchanov, A. Richter: Design of complex large-scale photonic integrated circuits (PICs) based on ring-resonator structures, in *Proc. OPTO Photonics West 2011*, paper 7933-29.

[4] S. F. Mingaleev, K. Busch: Scattering matrix approach to large-scale photonic crystal circuits, *Opt. Lett.* 28, 619–621 (2003).

[5] D. Hermann, M. Schillinger, S.F. Mingaleev, K. Busch: Wannier-function based scattering-matrix formalism for photonic crystal circuitry, *J. Opt. Soc. Am. B*, 25(2), 202-209 (2008).

[6] *VPIcomponentMakerTMPhotonic Circuits User's Manual*, Version 8.6, CMC-UM01-01 11054 (2011).

[7] S. Akiyama, T. Kurahashi, T. Baba, N. Hatori, T. Usuki, T. Yamamoto: Slow-light silicon Mach-Zehnder modulator based on cascaded ring resonators, in *Proc. CLEO/QELS*, paper CTuHH5 (2010).

[8] A. Yariv: Universal relations for coupling of optical power between microresonators and dielectric waveguides, *Elec. Lett.* 36 (4), 321-322 (2000).

[9] V. Van et al.: All-optical nonlinear switching in GaAs-AlGaAs microring resonators, *IEEE Photonics Technol. Lett*., vol. 14, no. 1, pp. 74-76 (2002).

[10] L. Zimmermann, et al.: C-Band optical 90 -hybrids based on silicon-on-insulator 4x4 waveguide couplers, *IEEE Photonics Technol. Lett*., vol. 21, no. 3, 2009.

[11] H.-G. Bach, A. Matiss, C.C. Leonhardt, R. Kunkel, D. Schmidt, M. Schell, A. Umbach: Monolithic 90°hybrid with balanced PIN photodiodes for 100 Gbit/s PM-QPSK receiver applications, *Digest Optical Fiber Commun. (OFC 2009)*, March 22-26, 2009, San Diego, California, USA, paper OMK5.

[12] L. B. Soldano and E. C. M. Pennings: Optical multimode interference devices based on self-imaging: Principles and applications, *J. Lightwave Technol*., vol. 13, pp. 615-627, 1995.

[13] A. Rigny, A. Bruno, H. Sik: Multigrating method for flattened spectral response wavelength multi/demultiplexer, *Electron. Let*t. 33, 1701-1702 (1997).